TECHNICAL NOTE

D-974

COMPARISON OF EXPERIMENTAL AND THEORETICAL STATIC AEROELASTIC LOADS AND DEFLECTIONS OF A THIN 45° DELTA WING IN SUPERSONIC FLOW

By Floyd V. Bennett

Langley Research Center
Langley Air Force Base, Va.

NATIONAL AERONAUTICS AND SPACE ADMINISTRATION

WASHINGTON October 1961

NATIONAL AERONAUTICS AND SPACE ADMINISTRATION

TECHNICAL NOTE D-974

COMPARISON OF EXPERIMENTAL AND THEORETICAL STATIC AEROELASTIC LOADS AND DEFLECTIONS OF A THIN 45° DELTA WING IN SUPERSONIC FLOW

By Floyd V. Bennett

SUMMARY

Wind-tunnel data showing the effects of static aeroelasticity for a thin 45° delta wing in supersonic flow are presented and compared with theory in the Mach number range 1.30 to 4.00. Calculated deformations, normal-force coefficients, and pitching-moment coefficients based on a linearized potential theory for subsonic leading edges at a Mach number of 1.30 and a linearized potential theory for supersonic leading edges at Mach numbers of 1.64, 3.00, and 4.00 are shown to compare favorably with the wind-tunnel results. Calculations of these same deformations and coefficients based on piston theory are shown to compare satisfactorily with experiment at a Mach number of 4.00 but not so well at a Mach number of 3.00. A factor modification of piston theory is suggested which improves the correlation of these results with experiment and also with the potential-theory results.

Although bending-moment coefficients were measured, the accuracy was not good enough to justify drawing any conclusions on this basis. Also, the effect of dynamic pressure on the static aeroelastic results is shown to decrease with Mach number.

INTRODUCTION

The elastic deformation of an aircraft under steady airload can modify the load distribution. For configurations such as supersonic transports and bombers, deformations may take place in the chord direction as well as in the more usual span direction. Although several theories are available for calculating these static aeroelastic effects (refs. 1 and 2), very little experimental verification and evaluation are available (ref. 2). Thus, in order to add to these experimental data and to obtain some results by which calculation procedures can be evaluated, a wind-tunnel investigation was undertaken.

A solid thin 45° delta wing of double-wedge cross section was tested at low, medium, and high dynamic pressures (250 to 2,000 lb/sq ft) at Mach numbers of 1.30, 1.64, 3.00, and 4.00. Static deformations, total normal force, pitching moment, and bending moment were measured. The purpose of this report is to present these experimental results and to present a comparison with calculated results for an evaluation of the theories used.

The calculations are based on the influence-coefficient method of analysis. The theories used to calculate the aerodynamic pressure distributions are (1) the linearized potential theory of reference 3 for subsonic leading edges, (2) the linearized potential theory of reference 4 for supersonic leading edges, and (3) the piston theory of reference 5. Some of the results of this study have been reported in reference 6, which presents a survey of the effects of aeroelasticity on stability and control.

SYMBOLS

A	area of wing segment
a	deformation coefficient (see eq. (3))
$\bar{a}$	average of a
$b/2$	wing semispan
C_{B_α}	coefficient of bending moment at tunnel wall $\left(\bar{y}_B = -0.0625\right)$ per unit angle of attack, $M_B/qSc_r\alpha$
C_{m_α}	coefficient of pitching moment about axis at $\bar{x}_p = 0.458$ per unit angle of attack, $M_p/qSc_r\alpha$
C_{N_α}	normal-force coefficient per unit angle of attack, $N/qS\alpha$
c_r	root chord
h_i	displacement at ith station
M	Mach number
M_B	aerodynamic bending moment at tunnel wall $\left(\bar{y}_B = -0.0625\right)$

M_p	aerodynamic pitching moment about axis at $\bar{x}_p = 0.458$
N	normal aerodynamic force
N_a	derivative of normal aerodynamic force with respect to a
N_z	derivative of normal aerodynamic force with respect to z
N_α	derivative of normal aerodynamic force with respect to angle of attack
Δ_p	differential pressure
q	dynamic pressure
S	total wing area
V	velocity of airstream
x,y	distances in the X- and Y-directions, respectively (see fig. 5)
X,Y,Z	coordinate axes (fig. 5)
$\bar{x} = x/c_r$	
x_p	x-distance to experimental pitch axis
$\bar{x}_p = x_p/c_r$	
$\bar{y} = \dfrac{y}{b/2}$	
y_B	y-distance to experimental bending-moment axis
$\bar{y}_B = \dfrac{y_B}{b/2}$	
z	deflection due to static aeroelasticity in Z-direction, positive down (see fig. 5)
α	rigid angle of attack
$\beta = \sqrt{M^2 - 1}$	
δ	structural influence coefficient (see eq. (1))

Subscripts:

i,j	refers to ith and jth station or matrix element, respectively
a	refers to derivative with respect to a
α	refers to derivative with respect to α

Matrix notation:

$\{ \}$	column matrix
$[\ ]$	square matrix
$\lceil \ \rfloor$	diagonal matrix

EXPERIMENT

Scope of Tests

Static aeroelastic normal deflections, normal aerodynamic forces, pitching moments, and bending moments were measured on a 45° triangular wing in supersonic flow. Conditions were investigated at four Mach numbers, 1.30, 1.64, 3.00, and 4.00. The angle of attack was varied from 2° to 10° at each Mach number. The dynamic pressure was varied from low to medium to high (from approximately 250 to 2,000 lb/sq ft, except at $M = 4.00$ where the maximum value of q attainable was 1,000 lb/sq ft) for each Mach number and angle of attack.

Description of Model and Apparatus

The test model is a 45° delta wing, a photograph of which is shown in figure 1. The root chord and semispan are 6 inches each. The airfoil is a double wedge with a thickness of 2 percent of the local chord parallel to the airstream. The wing is solid and is constructed from Type 416 stainless steel which was heat treated to a yield strength of 95,000 lb/sq ft.

The model was tested in the Langley 9- by 18-inch supersonic aeroelasticity tunnel. This tunnel is of the blowdown type with 2 to 10 seconds of running time. The test medium was air. The wing was cantilever mounted in the tunnel as shown in the photograph in figure 2. Notice the faired semicircular body (the radius is 0.375 inch) at the wing root. This faired body is attached to the tunnel wall and the wing extends through it. Thus, only the wing is attached to a strain-gage balance. The faired body is used to cut down on tunnel-wall boundary-layer interference on the wing.

Measurements of total normal force, pitching moment, and bending moment were recorded by an oscillograph during the entire tunnel operation. A camera was used to take double-exposure photographs showing the wing in the deformed and undeformed positions. (For example, see fig. 3.) The static aeroelastic deflections were measured from these photographs as described in appendix A.

Structural Characteristics of Model

The structural characteristics of the wing were measured in the form of influence coefficients. A structural influence coefficient δ_{ij} is defined as the deflection at station i due to a unit static load applied at station j. In the present instance the influence coefficients were measured by means of differential transformers (ref. 7) at 28 stations. The locations of these stations are shown in figure 4. The matrix of influence coefficients is given in table I.

Test Procedure

A photographic procedure was used to determine the wing deformations. The first step of this procedure was to paint a series of dashed white lines on the wing surface in order to locate properly points at which measurements were desired, as shown in figure 1. Next, the model was mounted in the test section, attached to the strain-gage balance, and rotated to a specified angle of attack. Then, just prior to the test run, a photograph was taken of the wing in this undeformed position, as in figure 2. Next, the tunnel was run at a specified Mach number and q condition. When the desired q condition was established in the tunnel, another photograph was taken of the wing in the now-deformed position. This photograph was taken on the same film as was the one showing the undeformed position of the wing, thus creating a double-exposure negative, as in figure 3. The purpose of the double-exposure negative is to determine the normal deflection. The procedure for obtaining these deflections is described in appendix A.

In order to correlate the continuous oscillograph record of wing force and moments with the deflections measured at only one instant during the test, a trigger mechanism was set up to mark the oscillograph record when the camera was operated. The tunnel was next run at a different dynamic pressure keeping the angle of attack and Mach number constant. After running the tunnel at low, medium, and high values of q, the wing was rotated to the next angle of attack and tested anew.

Finally, when the ranges of q and α were completed, the nozzle of the tunnel was changed in order to test the wing at the next Mach number condition.

Test Results

The test variables, Mach number, angle of attack, and dynamic pressure, are given in table II along with the coefficients of total normal aerodynamic force, pitching moment, and bending moment. The static aeroelastic deflections normal to the wing determined from the wind-tunnel tests are listed in table III. The pitch axis is located at $\bar{x}_p = 0.458$ and the bending moment is taken about an axis located at $\bar{y}_B = -0.0625$. (See fig. 5.)

ANALYSIS

In this section a brief description of the influence-coefficient method of analysis for calculating the effects of static aeroelasticity on a thin plate wing in supersonic flow is presented. The method of solution of the matrix equation of equilibrium is shown to be dependent on the type of aerodynamic theory used. In this report two types of solutions are discussed briefly.

Equation of Equilibrium

According to the influence-coefficient method, the deflection z_i of a point x_i,y_i on the wing subjected to discrete forces N_j acting normal to the wing surface in the Z-direction can be determined from the matrix equation

$$\left\{z\right\} = \left[\delta\right]\left\{N\right\} \tag{1}$$

where δ is a matrix of structural influence coefficients. The influence coefficient δ_{ij} is defined as the deflection at station i due to a unit normal force at station j. (See fig. 5.) This method requires that the wing be segmented as illustrated by the dashed regions in the figure and that the loads be concentrated at the influence stations located within each segment. The manner in which the wing was segmented for the present investigation and the locations of the influence stations are shown in figure 4.

For the static aeroelastic problem the only normal forces acting on the wing are (1) the aerodynamic force on the rigid wing at a preset angle of attack, and (2) the aerodynamic force due to the wing deforming statically; that is,

$$\left\{N\right\} = \alpha \left\{N_\alpha\right\} + \left[N_z\right] \left\{z\right\} \tag{2}$$

For the present problem the derivatives of the normal aerodynamic force N_α and N_z are determined by three different theories: (1) the linearized potential theory for subsonic leading edges of reference 3, (2) the linearized potential theory for supersonic leading edges of reference 4, and (3) the piston theory of reference 5. The solution of the equation of equilibrium is dependent on the type of aerodynamic theory used; thus, two methods of solution will be discussed briefly: (1) the solution using the potential theories, and (2) the solution using piston theory.

Solution using the potential theories.- The linearized potential theories of references 3 and 4 are limited to triangular planforms with zero thickness. For the subsonic leading edge of reference 3 the wing is assumed to be deforming harmonically with amplitude approximated by a quadratic expression for a surface. The velocity potential is obtained in the form of a power series of the frequency of oscillation. For the static aeroelastic problem this frequency of oscillation is zero. In the supersonic leading-edge theory of reference 4 only the steady-state solution is given with the deformation approximated by a power series in the surface variables limited to the first power in x and the third power in y.

In the present problem the wing displacement used in both potential theories is assumed to be

$$h_i = \alpha x_i + a x_i y_i^2 \tag{3}$$

where the first term is the displacement due to the rigid angle of attack and the second term is a first-order approximation for the deflection due to static aeroelasticity. A potential is then determined for each type of displacement from which the force derivatives are found. The expressions for these normal-force derivatives are given in appendix B for the subsonic-leading-edge case and in appendix C for the supersonic-leading-edge case. On the basis of this assumed description of the static aeroelastic deflection $\left(a x_i y_i^2\right)$, equation (2) becomes

$$\left\{N\right\} = \alpha \left\{N_\alpha\right\} + a \left\{N_a\right\} \tag{4}$$

Substituting $ax_iy_i^2$ for z in equation (1) and combining this equation with equation (4) gives, finally,

$$a\left\{\left\{xy^2\right\} - \left[\delta\right]\left\{N_a\right\}\right\} = \alpha\left[\delta\right]\left\{N_\alpha\right\} \tag{5}$$

The equations represented by equation (5) can now each be solved independently for a at each station. Since a was assumed to be a constant, then any variation in a as determined from each of the equations is averaged out before determining the static aeroelastic deflections and loads; that is,

$$\left\{z\right\} = \bar{a}\left\{xy^2\right\} \tag{6}$$

and

$$\left\{N\right\} = \alpha\left\{N_\alpha\right\} + \bar{a}\left\{N_a\right\} \tag{7}$$

Once $\left\{N\right\}$ has been determined the pitching and bending moments may be obtained from the following expressions:

$$M_p = \sum_i \left(x_i - x_p\right)N_i \tag{8}$$

$$M_B = \sum_i \left(y_i - y_B\right)N_i \tag{9}$$

Since there is an analytical expression for the deflections, then the forces and moments could be obtained by exact integration of the pressure over the surface. This procedure was followed for the subsonic-leading-edge case (see appendix B); however, for the supersonic-leading-edge case the effort required to perform the exact integrations was considered excessive and numerical integration was used.

Solution using piston theory.- The basic assumptions of piston theory are high Mach numbers $\left(M^2 >> 1\right)$ and thin wings. Unlike the linearized potential theories this theory allows for the inclusion of airfoil shape and thickness effects. For the present problem expressions for the normal-force derivatives as determined by piston theory are given in appendix D.

For this theory it is not necessary to assume an analytical expression for the deflection shape; therefore, substituting equation (2) into equation (1) gives

$$\left\{z\right\} = \alpha\left[\delta\right]\left\{N_\alpha\right\} + \left[\delta\right]\left[N_Z\right]\left\{z\right\} \tag{10}$$

This equation may be solved for the static deflection $\left\{z\right\}$ by iteration. Once $\left\{z\right\}$ has been obtained the normal static load is found from equation (2) and, finally, the moments are obtained from equations (8) and (9).

RESULTS AND DISCUSSION

This section is divided into two parts. In the first part a comparison is made between experimental and calculated deformations of the lifting surface. The second part presents a similar comparison for the coefficients of total normal force, pitching moment, and bending moment per unit angle of attack.

Deformations

Since the lifting surface is of the plate type, the deformations will be plotted along both the chordwise and spanwise directions. The local chord lines and the span lines (which are lines of constant fractions of local chord) on which the deformation plots are based are shown in figure 6. Typical plots of the experimental and calculated deformations for the four Mach number conditions are shown in figure 7. In general, the agreement between experiment and the appropriate potential-theory results is satisfactory for all Mach numbers considered. The calculations were based on the subsonic-leading-edge theory for $M = 1.30$ and on the supersonic-leading-edge theory for the higher Mach numbers. On the basis of this comparison, it is expected that these potential theories should give results of corresponding accuracy when applied to similar lifting surfaces.

Piston theory, used only for $M = 3.00$ and $M = 4.00$ (figs. 7(c) and (d)), yields satisfactory agreement with experiment at $M = 4.00$ but is not so good, deviating by 20 percent in some instances, at $M = 3.00$. However, the piston-theory results at $M = 3.00$ are considered to be accurate enough for use in trend studies where many calculations are involved. In such studies piston theory becomes very attractive due to its simplicity. (Compare the equations of appendix C with those of appendix D.) As stated previously, piston theory includes finite-thickness effects; however, since the wing is only 2 percent thick, no detailed conclusions regarding this effect are made.

Normal-Force and Moment Coefficients

By using the calculated deflections the coefficients of normal force, pitching moment, and bending moment were calculated for each Mach number condition. The pitch axis is located at $\bar{x}_p = 0.458$ and the bending-moment axis is located at $\bar{y}_B = -0.0625$ (at the tunnel wall). (See fig. 5.) Comparisons between the experimentally and theoretically determined force and moment coefficients are given in the following subsections.

Normal-force coefficient.- The experimental and theoretical values of the coefficient of normal force per unit angle of attack are shown in figure 8 as a function of dynamic pressure. The difference between theory and experiment is generally within 10 percent; however, it should be pointed out that the difference between experiment and piston theory at $M = 3.00$ is of the order of 15 percent. However, by a slight modification of piston theory the correlation with experiment can be improved. That is, inserting $1/\beta$ for the $1/M$ factor in the expression for differential pressure (see appendix D) results in an increase in the normal-force coefficient. This modification tends to aline piston theory with linearized potential theory and even with some second-order theories, such as that of Van Dyke (ref. 8). In fact, the normal-force coefficient predicted by this modification for a rigid wing with supersonic leading edges $(4/\beta)$ is identical to that predicted by linearized potential theory. On this basis, then, the calculated rigid results shown in figure 8 would be identical to the potential-theory results at $M = 3.00$ and 4.00 (and even at $M = 1.64$ if piston theory had been used here). The flexible results would be increased approximately in the same proportion as the rigid results (reducing the discrepancies from 15 to 10 percent at $M = 3.00$); the increase in the flexible results would not be identical to the increase in the rigid results because the deformations used in the calculation of the flexible loads would be slightly different due to the modification. As regards the evaluation of the theories, the comparisons made in figure 8 support the conclusions made regarding the comparison of deformations.

In order to indicate the loss in normal-load coefficient due to static aeroelasticity, the rigid results shown in figure 8 are used as reference values. By comparison with these rigid results, the effects of flexibility are shown to be large at the lower Mach numbers (20 percent for $M = 1.30$ at $q = 1{,}000$ lb/sq ft and increases as q increases). As Mach number is increased, however, the effect of flexibility decreases (only 4 percent for $M = 4.00$ at $q = 1{,}000$ lb/sq ft). The same trend can be established from the experimental results by extrapolating q to zero and using this result as a reference value.

Pitching-moment coefficient.- The coefficient of pitching moment per unit angle of attack based on theory and experiment is plotted in figure 9 against the dynamic pressure. The agreement and trends of the results are about the same as for C_{N_α}; however, at $M = 1.30$ the agreement between experiment and theory is only fair. Also, at the higher Mach numbers piston theory is in better agreement with experiment than is the potential theory. Although the wing is only 2 percent thick it seems that the finite-thickness effect, present in piston theory and not in the potential theory, causes a shift in the prediction of the chordwise location of center of pressure and thus has more of an effect on C_{m_α} than on C_{N_α}. If piston theory were modified as before, the results would still be in better agreement with the experimental results than are the potential-theory results. The modified piston theory predicts, for a rigid wing ($q = 0$), $C_{m_\alpha} = -0.284$ per radian at $M = 3.00$ and $C_{m_\alpha} = -0.206$ per radian at $M = 4.00$ or roughly halfway between the piston- and potential-theory results.

A comparison of the flexible and rigid potential-theory results again indicates a large effect due to flexibility at the low Mach numbers (as much as 30 percent for $M = 1.30$ at $q = 1,000$ lb/sq ft) and a decrease in this effect as the Mach number is increased (7 percent for $M = 4.00$ at $q = 1,000$ lb/sq ft).

Bending-moment coefficient.- In figure 10 the coefficient of bending moment per unit angle of attack is plotted against the dynamic pressure. There is so much scatter in the experimental values of C_{B_α} (which is considered to be due to balance insensitivity) that no attempt is made to assess the theoretical results; however, the overall trends of the experimental and theoretical results with dynamic pressure are in agreement. These trends are the same as those in figures 8 and 9 for C_{N_α} and C_{m_α}, respectively.

As a matter of interest, the modified piston theory would again predict results between those predicted by piston theory and potential theory (for the rigid wing, $C_{B_\alpha} = 0.561$ per radian at $M = 3.00$ and $C_{B_\alpha} = 0.406$ per radian at $M = 4.00$). Also, a comparison of the flexible and rigid results again indicates a larger effect of flexibility at the lower Mach numbers than at the higher values.

CONCLUDING REMARKS

Static aeroelastic wind-tunnel data for a thin 45° delta wing in supersonic flow have been presented and compared with theory in the Mach number M range 1.30 to 4.00. Three theoretical procedures were used: (1) a linearized potential theory for subsonic leading edges at $M = 1.30$; (2) a linearized potential theory for supersonic leading edges at $M = 1.64$, 3.00, and 4.00; and (3) a piston theory at $M = 3.00$ and $M = 4.00$. Results presented are normal deflections, normal-force coefficient, pitching-moment coefficient, and bending-moment coefficient.

In general, calculations of the deformations, normal-force coefficients, and pitching-moment coefficients based on the potential theories have been shown to agree favorably with the wind-tunnel results. Calculations of these same results based on piston theory have been shown to compare satisfactorily with experiment at $M = 4.00$ but not so well at $M = 3.00$. However, a suggested factor modification in piston theory can improve the correlation with experiment. This modification tends to aline piston theory with linearized potential theory and even with some second-order theories, such as that of Van Dyke.

Agreement between theoretical and experimental bending-moment coefficients was shown to be poor. However, an assessment of the theories on this basis was not made inasmuch as the experimental results were considered to be inaccurate due to balance insensitivity.

Langley Research Center,
National Aeronautics and Space Administration,
Langley Air Force Base, Va., August 30, 1961.

APPENDIX A

PROCEDURE FOR MEASURING DEFLECTIONS

The procedure for measuring deflections was as follows. First, white lines were painted on the wing surface. These lines were broken at the stations at which values of deflections were desired. (See fig. 1.) Second, a camera was set up as indicated in the following sketch:

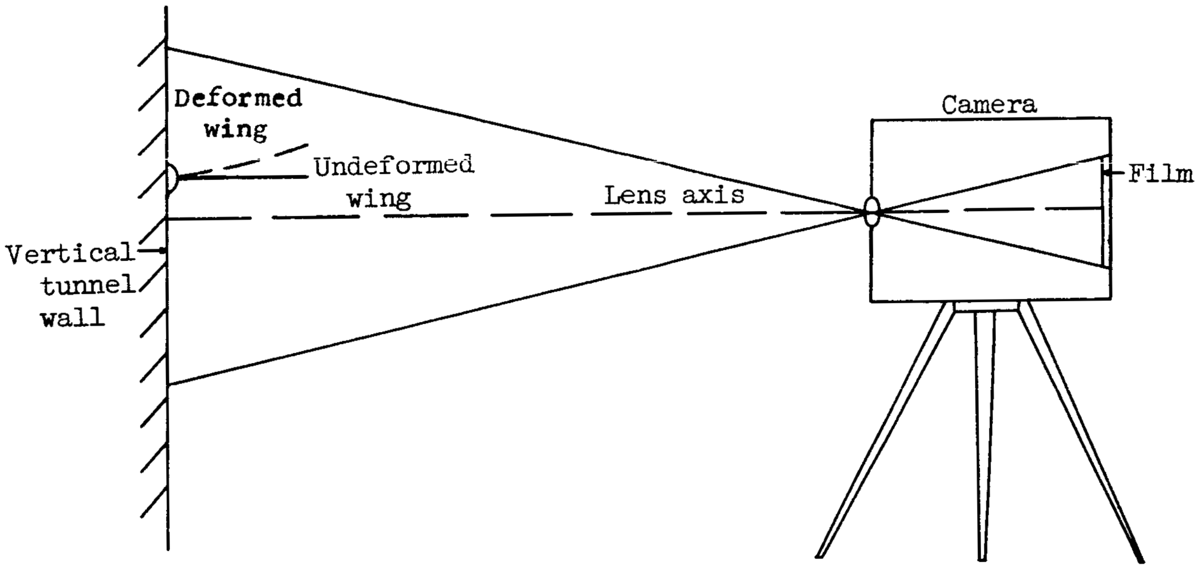

Note that the lens axis is below the wing and perpendicular to the vertical tunnel wall. This axis is below the wing in order to distinguish between the white lines at different span stations. (See fig. 2.) It is perpendicular to the vertical tunnel wall in order to present an undistorted view of normal deflections (normal to the wing local chords in the undeflected position). Third, a double-exposure negative was made showing the wing in the undeflected position before each run with the deflected wing superimposed during each run; for example, see figure 3. Finally, this double-exposure negative was magnified and the distances between the broken white lines in the disturbed and undisturbed positions were measured and multiplied by a conversion factor in order to determine the actual deflection. This conversion factor is simply the ratio of the actual local chord length to the local chord length as measured from the magnified negative. This factor is based on the assumption that the camera distorts distances linearly and equally in both the normal and chordwise directions. That is,

$$z = z_c\left(\frac{c}{c_c}\right)$$

where

z	actual normal deflection, in.
z_c	normal deflection measured on negative
c	actual length of lines on wing, in.
c_c	length of lines on wing measured on negative

APPENDIX B

LINEARIZED POTENTIAL THEORY FOR SUBSONIC LEADING EDGES

In this appendix application of the linearized potential theory of reference 3 for subsonic leading edges is made to the static aeroelastic problem of this report. The equations for the coefficients of normal load, pitching moment, and bending moment for a 45° triangular wing deforming statically are presented.

The theory is limited to thin triangular wings (thickness is assumed to be zero) in supersonic flow with subsonic leading edges undergoing harmonic motion. The amplitude of the deformations is assumed to be represented by a quadratic expression for a surface. The velocity potential is obtained in the form of a power series in terms of the frequency of oscillation. For the static aeroelastic problem this frequency is zero.

For the present problem the displacement of the wing is assumed to be of the form (see the axis system, fig. 5)

$$h_i = \alpha x_i + a x_i y_i^2$$

The velocity potentials are then obtained from reference 3 for two angles of attack, one equal to a constant α and one equal to $a y_i^2$. On this basis, then, the normal aerodynamic force can be written in matrix notation as

$$\left\{N\right\} = \alpha\left\{N_\alpha\right\} + a\left\{N_a\right\}$$

$$\left\{N_\alpha\right\} = \frac{4q}{E'}\left[A\right]\left\{\frac{\bar{x}}{\sqrt{\bar{x}^2 - \bar{y}^2}}\right\}$$

$$\left\{N_a\right\} = \frac{-4\left(\frac{b}{2}\right)^2}{\beta^2}\left[A\right]\left\{3b_0\bar{x}^3 + \left(b_1\beta^2 - 2b_0\right)\bar{x}\bar{y}^2\right\}$$

where b_0 and b_1 are constants with respect to the surface coordinates which depend on M and the wing apex angle (ref. 3). (For the 45° delta wing at $M = 1.3$, $b_0 = 0.025465$ and $b_1 = 0.21947$.) The symbol E' represents a complete elliptic integral of the second kind with the modulus $\sqrt{1 - \beta^2}$. The area of the wing segments is tabulated in figure 4 for the wing under study.

Due to the discrete nature of the influence coefficients it is necessary to define the aerodynamic forces at discrete stations in order to determine the deflections; however, once the deflection has been determined (in this case the average value of the deflection coefficient $\bar{a}$), the aerodynamic pressures may be integrated analytically to determine the total aerodynamic force as

$$N = \iint_S \left(\alpha \Delta p_\alpha + \bar{a} \Delta p_a\right) dx\, dy$$

$$= \frac{q\left(\frac{b}{2}\right)^2 \pi}{E'} \alpha - \frac{q\bar{a}\left(\frac{b}{2}\right)^4 \pi}{\beta^2}\left(b_0 + \frac{1}{4} b_1 \beta^2\right)$$

Thus, the coefficient of normal force is

$$C_{N_\alpha} = \frac{N}{qS\alpha} = \frac{2\pi}{E'} - \frac{2\pi\bar{a}\left(\frac{b}{2}\right)^2}{\beta^2 \alpha}\left(b_0 + \frac{1}{4} b_1 \beta^2\right)$$

Similarly, the pitching-moment and bending-moment coefficients are, respectively,

$$C_{m_\alpha} = \frac{-4\pi}{E'}\left(\frac{1}{3} - \frac{1}{2}\bar{x}_p\right) + \frac{2\pi c_r^2 \bar{a}}{\beta^2 \alpha}\left(b_0 + \frac{1}{4} b_1 \beta^2\right)\left(\frac{4}{5} + \bar{x}_p\right)$$

$$C_{B_\alpha} = \frac{4}{E'}\left(\frac{2}{3} - \bar{y}_B \pi\right) + \frac{4 c_r^2 \bar{a}}{\beta^2 \alpha}\left[\frac{2}{3}\left(b_0 + \frac{2}{5} b_1 \beta^2\right) - \frac{\pi}{2}\bar{y}_B\left(b_0 + \frac{1}{4} b_1 \beta^2\right)\right]$$

APPENDIX C

LINEARIZED POTENTIAL THEORY FOR SUPERSONIC LEADING EDGES

In this appendix application of the linearized potential theory of reference 4 for supersonic leading edges is made to the static aeroelastic problem of this report. The equations for the normal aerodynamic loads for a 45° triangular wing deforming statically are presented.

The theory is limited to thin triangular wings (thickness is assumed to be zero) in steady supersonic flow with supersonic leading edges. The deformations are assumed to be represented by a power series in the surface variables limited to the first power in x and the third power in y.

For the present problem the displacement of the wing is assumed to be of the form (see the axis system, fig. 5)

$$h_i = \alpha x_i + a x_i y_i^2$$

The velocity potentials are then obtained from reference 4 for two angles of attack, one equal to a constant α and one equal to $a y_i^2$. On this basis, then, the normal aerodynamic force can be written in matrix notation as

$$\left\{N\right\} = \alpha\left\{N_\alpha\right\} + a\left\{N_a\right\}$$

where

$$\left\{N_\alpha\right\} = \left[A\right]\left\{\Delta p_\alpha\right\}$$

$$\left\{N_a\right\} = \left[A\right]\left\{\Delta p_a\right\}$$

The areas of the wing segments are tabulated in figure 4 for the wing under study. The elements of the matrices of the differential pressure derivatives are as follows:

(1) For stations ahead of the Mach line,

$$\Delta p_\alpha = \frac{4}{\sqrt{\beta^2 - 1}}$$

$$\Delta p_a = \frac{-2(b/2)^2}{(\beta^2 - 1)^{5/2}}\left[2(\beta^2\bar{y} - \bar{x})^2 + \beta^2(\bar{x} - \bar{y})^2\right]$$

(2) For stations rearward of the Mach line,

$$\Delta p_\alpha = \frac{4}{\pi\sqrt{\beta^2 - 1}}\left(\theta_1 + \theta_2\right)$$

$$\Delta p_a = \frac{-2(b/2)^2}{(\beta^2 - 1)^{5/2}}\left\{\left[2(\beta^2\bar{y} - \bar{x})^2 + \beta^2(\bar{x} - \bar{y})^2\right]\theta_1\right.$$

$$\left. + \left[2(\beta^2\bar{y} + \bar{x}) + \beta^2(\bar{x} + \bar{y})^2\right]\theta_2 - 6\bar{x}\sqrt{(\beta^2 - 1)(\bar{x}^2 - \beta^2\bar{y}^2)}\right\}$$

where

$$\theta_1 = \cos^{-1}\left[\frac{\bar{x} - \beta^2\bar{y}}{\beta(\bar{x} - \bar{y})}\right]$$

$$\theta_2 = \cos^{-1}\left[\frac{\bar{x} + \beta^2\bar{y}}{\beta(\bar{x} + \bar{y})}\right]$$

APPENDIX D

PISTON THEORY

In this appendix application of piston theory (ref. 5) is made to the static aeroelastic problem of this report. The equations for the normal aerodynamic forces for a 45° delta wing deforming statically are presented.

The theory is limited to thin wings in supersonic flow at high Mach number, where $\sqrt{M^2 - 1} \approx M$. Unlike the linearized potential theories, this theory allows for the inclusion of the effects of airfoil shape and thickness. The differential pressure at the ith station Δp_i is given by second-order piston theory for symmetrical airfoils as

$$\Delta p_i = \frac{4q}{M}\left[1 + \frac{M(\gamma + 1)}{2} Y_s'(x_i)\right]\frac{w(x_i)}{V}$$

where

γ ratio of specific heats of medium

$w(x_i)$ downwash velocity at station i

$Y_s(x_i)$ defines the contour of the upper wing surface

The prime denotes a derivative with respect to x. In this theory the axis system is defined by figure 5.

For the static aeroelastic problem

$$w(x_i) = V\left(\alpha + z_i'\right)$$

In order to determine the force N_i at station i, Δp_i is integrated over the x-distance of the segment of area associated with station i and multiplied by a constant strip width s_i. (For the present problem these segments are shown in fig. 4.) Thus, at station i,

$$N = \frac{4q}{M}\left[A\alpha + s\left(\int z'dx\right) + \frac{M(\gamma + 1)}{2}\alpha s \int Y_s'(x)dx + \frac{M(\gamma + 1)}{2}s \int Y_s'(x)z'dx\right]$$

or in matrix notation

$$\left\{N\right\} = \frac{4q\alpha}{M}\left\lceil \left\lceil A \right\rfloor + \frac{M(\gamma + 1)}{2}\left\lceil s \right\rfloor \left\lceil S_Y \right\rfloor \right\rfloor \left\{1\right\}$$

$$+ \frac{4q}{M}\left\lceil s \right\rfloor \left[\left[S_z\right] + \frac{M(\gamma + 1)}{2}\left[S_{Y,z}\right]\right]\left\{z\right\}$$

where

$\left\lceil S_Y \right\rfloor$ integrating matrix, $\int Y_s'(x)dx$

$\left[S_z\right]$ integrating matrix, $\int z'dx$

$\left[S_{Y,z}\right]$ integrating matrix, $\int Y_s'(x)z'dx$

Comparing the preceding equation with equation (2) gives

$$\left\{N_\alpha\right\} = \frac{4q}{M}\left\lceil \left\lceil A \right\rfloor + \frac{M(\gamma + 1)}{2}\left\lceil s \right\rfloor \left\lceil S_Y \right\rfloor \right\rfloor \left\{1\right\}$$

and

$$\left[N_z\right] = \frac{4q}{M}\left\lceil s \right\rfloor \left[\left[S_z\right] + \frac{M(\gamma + 1)}{2}\left[S_{Y,z}\right]\right]$$

For the wing studied the areas of the wing segments are tabulated in figure 4. The equation of the upper surface is for $0 \leqq x \leqq c/2$

$$Y_s = \tau x$$

and for $c/2 \leqq x \leqq c$

$$Y_s = \tau(c - x)$$

where

τ	thickness ratio, fraction of local chord (0.02)
c	local chord

Numerical values of the remaining matrices are given as follows, in inches:

$$\begin{bmatrix} s \end{bmatrix} = \begin{bmatrix} 1 \end{bmatrix}$$

$$\begin{bmatrix} S_Y \end{bmatrix} = \tau \begin{bmatrix} \begin{bmatrix} S_Y^{(1)} \end{bmatrix} & & & & & \\ & \begin{bmatrix} S_Y^{(2)} \end{bmatrix} & & & & \\ & & \begin{bmatrix} S_Y^{(3)} \end{bmatrix} & & & \\ & & & \begin{bmatrix} S_Y^{(4)} \end{bmatrix} & & \\ & & & & \begin{bmatrix} S_Y^{(5)} \end{bmatrix} & \\ & & & & & \begin{bmatrix} S_Y^{(6)} \end{bmatrix} \end{bmatrix}$$

where

$$\begin{bmatrix} S_Y^{(1)} \end{bmatrix} = \begin{bmatrix} 1.1 & & & & \\ & 1.1 & & & \\ & & 0 & & \\ & & & -1.1 & \\ & & & & -1.1 \end{bmatrix}$$

$$\left[S_Y^{(2)} \right] = \begin{bmatrix} 0.9 & & & & \\ & 0.9 & & & \\ & & 0 & & \\ & & & -0.9 & \\ & & & & -0.9 \end{bmatrix}$$

$$\left[S_Y^{(3)} \right] = \begin{bmatrix} 0.7 & & & & \\ & 0.7 & & & \\ & & 0 & & \\ & & & -0.7 & \\ & & & & -0.7 \end{bmatrix}$$

$$\left[S_Y^{(4)} \right] = \begin{bmatrix} 0.5 & & & & \\ & 0.5 & & & \\ & & 0 & & \\ & & & -0.5 & \\ & & & & -0.5 \end{bmatrix}$$

$$\left[S_Y^{(5)} \right] = \begin{bmatrix} 0.3 & & & & \\ & 0.3 & & & \\ & & 0 & & \\ & & & -0.3 & \\ & & & & -0.3 \end{bmatrix}$$

$$\left[S_Y^{(6)}\right] = \begin{bmatrix} 0.15 & & \\ & 0 & \\ & & -0.15 \end{bmatrix}$$

and

$$\left[S_z\right] = \begin{bmatrix} \left[S_z^{(1)}\right] & [0] & \cdot & \cdot & \cdot & [0] \\ [0] & \left[S_z^{(1)}\right] & \cdot & \cdot & \cdot & \cdot \\ \cdot & \cdot & \left[S_z^{(1)}\right] & \cdot & \cdot & \cdot \\ \cdot & \cdot & \cdot & \left[S_z^{(1)}\right] & \cdot & \cdot \\ \cdot & \cdot & \cdot & \cdot & \left[S_z^{(1)}\right] & [0] \\ [0] & \cdot & \cdot & \cdot & [0] & \left[S_z^{(2)}\right] \end{bmatrix}$$

where

$[0]$ square matrix of zeros

$$\left[S_z^{(1)}\right] = \frac{1}{1.6}\begin{bmatrix} -2.4 & 3.2 & -0.8 & 0 & 0 \\ -0.8 & 0 & 0.8 & 0 & 0 \\ 0.2 & -1.2 & 0 & 1.2 & -0.2 \\ 0 & 0 & -0.8 & 0 & 0.8 \\ 0 & 0 & 0.8 & -3.2 & 2.4 \end{bmatrix}$$

$$\left[S_z^{(2)}\right] = \frac{1}{1.28}\begin{bmatrix} -1.32 & 1.68 & -0.36 \\ -0.64 & 0 & 0.64 \\ 0.36 & 1.68 & 1.32 \end{bmatrix}$$

and

$$\left[S_{Y,z}\right] = \tau\begin{bmatrix} \left[S_{Y,z}^{(1)}\right] & [0] & \cdots & \cdot & [0] \\ [0] & \left[S_{Y,z}^{(1)}\right] & \cdot & \cdot & \cdot \\ \cdot & \cdot & \left[S_{Y,z}^{(1)}\right] & \cdot & \cdot \\ \cdot & \cdot & \cdot & \left[S_{Y,z}^{(1)}\right] & [0] \\ [0] & \cdot & \cdots & [0] & \left[S_{Y,z}^{(2)}\right] \end{bmatrix}$$

where

$$\left[S_{Y,z}^{(1)}\right] = \frac{1}{1.6}\begin{bmatrix} -2.4 & 3.2 & -0.8 & 0 & 0 \\ -0.8 & 0 & 0.8 & 0 & 0 \\ 0.2 & -1.2 & 2.0 & -1.2 & 0.2 \\ 0 & 0 & 0.8 & 0 & -0.8 \\ 0 & 0 & -0.8 & 3.2 & -2.4 \end{bmatrix}$$

$$\left[S_{Y,z}^{(2)}\right] = \frac{1}{1.28}\begin{bmatrix} -1.32 & 1.68 & -0.36 \\ -0.32 & 0.64 & -0.32 \\ -0.36 & 1.68 & -1.32 \end{bmatrix}$$

REFERENCES

1. Bisplinghoff, Raymond L., Ashley, Holt, and Halfman, Robert L.: Aeroelasticity. Addison-Wesley Pub. Co., Inc. (Cambridge, Mass.), c.1955.

2. Zisfein, Melvin B., Donato, Vincent W., and Farrell, Robert F.: Supersonic Aeroelastic Effects on Static Stability and Control. Part I - Aerodynamics. Vol. I, WADC Tech. Rep. 58-95, ASTIA Doc. No. AD 155739, U.S. Air Force, Dec. 1958.

3. Watkins, Charles E., and Berman, Julian H.: Velocity Potential and Air Forces Associated With a Triangular Wing in Supersonic Flow, With Subsonic Leading Edges, and Deforming Harmonically According to a General Quadratic Equation. NACA TN 3009, 1953.

4. Kainer, Julian H.: Equations for the Loading on Triangular Wings Having Supersonic Leading and Trailing Edges Due to Various Basic Twist Distributions. Jour. Aero. Sci., vol. 20, no. 7, July 1953, pp. 469-476.

5. Lighthill, M. J.: Oscillating Airfoils at High Mach Number. Jour. Aero. Sci., vol. 20, no. 6, June 1953, pp. 402-406.

6. Runyan, H. L., Pratt, K. G., and Bennett, F. V.: Effects of Aeroelasticity on the Stability and Control Characteristics of Airplanes. Presented to AGARD Specialists Meeting on Stability and Control (Brussels, Belgium), Apr. 10-14, 1961.

7. Macgeorge, W. D.: The Differential Transformer. [Preprint] 49-8-1, Instrument Soc. of America, Sept. 1949.

8. Van Dyke, Milton D.: A Study of Second-Order Supersonic Flow Theory. NACA Rep. 1081, 1952. (Supersedes NACA TN 2200.)

TABLE I.- MATRIX OF STRUCTURAL INFLUENCE COEFFICIENTS

[Since $\delta_{ij} = \delta_{ji}$ only half of matrix is listed]

Station	Structural influence coefficient, millionths of an inch per pound, at station -																											
	1	2	3	4	5	6	7	8	9	10	11	12	13	14	15	16	17	18	19	20	21	22	23	24	25	26	27	28
1	431																											
2	79	113																										
3	79	68	91																									
4	56	79	102	159																								
5	34	57	91	136	559																							
6	159	170	124	79	45	1,043																						
7	102	136	170	113	79	374	431																					
8	90	102	147	170	136	226	374	454																				
9	56	91	147	249	272	136	295	487	748																			
10	45	91	170	272	465	45	204	487	1,009	2,568																		
11	102	159	204	192	90	521	737	727	578	328	2,676																	
12	124	195	215	227	136	407	646	816	784	669	1,700	1,859																
13	91	136	204	170	238	318	578	918	1,042	1,111	1,360	1,799	2,063															
14	68	136	192	340	295	200	499	873	1,292	1,666	1,156	1,700	2,301	3,062														
15	34	102	182	363	408	124	465	907	1,543	2,336	873	1,587	2,473	3,662	6,075													
16	99	160	283	320	195	478	845	1,250	1,220	1,125	2,305	2,958	3,078	3,035	2,790	6,910												
17	91	185	261	351	257	400	807	1,185	1,424	1,400	2,150	2,850	3,360	3,685	3,835	6,090	6,652											
18	62	142	295	378	230	363	790	1,229	1,661	1,760	1,904	2,810	3,580	4,190	4,750	5,800	6,740	7,620										
19	75	142	242	412	335	260	710	1,270	1,665	2,100	1,685	2,730	3,674	4,760	5,800	5,480	6,940	8,313	9,797									
20	30	120	200	420	430	136	690	1,380	1,950	2,494	1,520	2,650	3,755	5,385	6,810	5,110	6,975	8,880	10,920	15,600								
21	84	166	310	442	333	453	1,000	1,636	1,916	1,848	2,638	3,888	4,730	5,366	5,617	8,585	10,330	11,405	11,945	12,000	23,430							
22	121	166	350	454	330	450	950	1,650	1,965	2,112	2,560	3,760	5,000	5,800	6,350	8,490	10,200	11,850	13,200	13,650	22,750	23,500						
23	87	155	300	480	390	300	960	1,645	2,160	2,290	2,490	3,750	5,110	6,140	6,990	8,500	10,400	12,390	14,300	15,350	22,750	24,720	24,930					
24	91	250	350	490	380	300	890	1,640	2,300	2,610	2,358	3,700	5,200	6,490	7,550	8,300	10,500	12,680	15,260	16,700	22,770	25,300	26,900	31,480				
25	91	150	340	550	420	340	950	1,724	2,380	2,730	2,190	3,720	5,215	6,803	8,180	8,010	10,650	13,200	16,000	18,500	22,550	26,300	30,400	35,200	43,000			
26	100	200	280	300	460	700	1,150	1,900	2,560	2,550	2,700	4,720	6,400	7,600	8,450	10,600	13,900	16,900	19,000	20,300	38,570	38,550	44,500	46,800	49,000	124,000		
27	100	200	400	600	460	295	1,120	2,000	2,800	3,010	2,870	4,560	6,450	8,130	9,100	10,800	14,900	16,500	19,500	21,600	23,900	38,000	43,400	48,500	53,200	127,000	141,100	
28	100	300	425	450	470	550	1,050	2,000	2,500	3,100	2,750	4,600	6,500	8,160	9,700	13,000	14,000	16,000	19,000	23,000	34,000	39,000	43,500	50,000	56,000	128,500	148,000	174,100

TABLE II.- EXPERIMENTAL LOAD RESULTS AND RUN VARIABLES

Run	M	α, deg	q, lb/sq ft	C_{N_α}, per radian	$-C_{m_\alpha}$, per radian	C_{M,B_α}, per radian
8	1.30	2	255	4.50	0.810	3.22
9		2	975	3.76	.627	1.99
10		2	1,555	3.58	.522	2.11
11		4	258	4.48	.770	2.76
12		4	549	3.95	.640	2.56
13		4	900	3.63	.588	2.05
14		6	249	4.41	.743	2.92
15		6	526	3.85	.648	2.29
16		8	255	4.27	.735	2.63
17		8	409	3.99	.670	2.37
22	1.64	2	295	3.57	.599	2.32
23		2	1,140	2.91	.490	1.70
24		2	1,988	2.36	.378	1.33
25		4	603	3.02	.543	1.81
26		4	352	3.26	.585	1.61
27		4	999	2.98	.485	1.66
28		6	320	3.30	.589	1.89
29		6	642	3.00	.522	1.72
30		8	311	3.23	.566	1.83
31		8	521	3.11	.538	1.67
34	3.00	3	583	1.44	.251	.625
35		3	1,040	1.41	.233	.781
36		3	2,063	1.38	.219	.619
37		6	231	1.52	.270	.828
38		6	1,055	1.40	.243	.700
39		6	2,130	1.36	.217	.660
40		9	233	1.57	.265	.938
41		9	870	1.45	.251	.777
42		9	2,020	1.36	.218	.649
48	4.00	3	268	1.14	.218	.760
49		3	489	1.06	.189	.584
50		3	987	.99	.187	.659
51		6	295	1.01	.198	.462
52		6	495	1.05	.190	.692
53		6	980	1.02	.189	.579
54		10	268	1.11	.215	.620
55		10	475	1.06	.201	.557
56		10	981	1.06	.191	.574

TABLE III.- EXPERIMENTAL DEFLECTION RESULTS

Run	Experimental deflection results, in., at station -																										
	1	2	3	4	5	6	7	8	9	10	11	12	13	14	15	16	17	18	19	20	21	22	23	24	25	26	27	28
8	0.000	0.000	0.000	0.000	0.000	0.004	0.004	0.004	0.004	0.004	0.006	0.009	0.013	0.013	0.016	0.018	0.023	0.025	0.027	0.030	0.041	0.043	0.047	0.050	0.048	0.079	0.084	0.088
9	.000	.000	.000	.000	.000	.004	.008	.012	.016	.016	.022	.028	.035	.038	.041	.055	.064	.068	.073	.080	.115	.123	.130	.137	.142	.223	.230	.238
10	.000	.000	.000	.000	.000	.008	.012	.016	.020	.024	.028	.038	.047	.057	.060	.080	.091	.098	.107	.112	.163	.173	.182	.188	.196	.302	.315	.325
11	.000	.000	.000	.000	.000	.000	.004	.008	.012	.012	.013	.019	.022	.022	.025	.034	.039	.043	.048	.052	.075	.079	.083	.086	.091	.141	.143	.147
12	.000	.000	.000	.000	.000	.004	.012	.016	.020	.020	.025	.032	.038	.044	.050	.064	.073	.080	.089	.096	.134	.144	.152	.159	.164	.251	.264	.272
13	.000	.000	.005	.005	.005	.008	.016	.024	.028	.032	.038	.047	.057	.063	.072	.091	.105	.114	.125	.135	.190	.203	.214	.224	.233	.351	.366	.378
14	.000	.000	.000	.000	.005	.000	.008	.012	.016	.016	.019	.025	.028	.035	.038	.046	.052	.059	.066	.073	.099	.105	.110	.119	.126	.170	.175	.184
15	.000	.000	.000	.005	.005	.004	.012	.020	.024	.028	.035	.044	.050	.060	.066	.087	.098	.107	.121	.130	.179	.192	.203	.211	.222	.332	.347	.360
16	.000	.000	.000	.005	.000	.000	.012	.016	.016	.020	.025	.028	.038	.044	.050	.059	.071	.075	.087	.093	.126	.135	.142	.150	.157	.216	.223	.232
17	.000	.000	.000	.005	.005	.008	.016	.020	.024	.028	.035	.044	.054	.063	.072	.089	.100	.114	.123	.135	.185	.196	.207	.221	.233	.343	.359	.368
22	.000	.000	.000	.000	.000	.000	.000	.000	.000	.000	.003	.006	.009	.013	.013	.016	.018	.018	.023	.025	.030	.032	.036	.037	.037	.061	.062	.065
23	.000	.000	.000	.000	.000	.004	.004	.008	.012	.016	.019	.022	.025	.032	.035	.046	.052	.055	.064	.066	.090	.098	.102	.109	.115	.162	.167	.174
24	.000	.000	.000	.000	.000	.004	.008	.016	.016	.024	.025	.032	.035	.044	.047	.059	.066	.075	.084	.089	.123	.127	.135	.142	.145	.212	.218	.226
25	.000	.000	.000	.000	.000	.004	.008	.012	.016	.016	.019	.022	.032	.035	.041	.050	.059	.064	.068	.078	.105	.110	.117	.123	.130	.191	.197	.209
26	.000	.000	.000	.000	.000	.000	.004	.012	.012	.012	.019	.022	.022	.025	.028	.034	.039	.043	.046	.050	.069	.073	.080	.083	.088	.127	.134	.141
27	.000	.000	.005	.005	.005	.008	.016	.020	.024	.028	.032	.038	.047	.057	.063	.078	.087	.096	.107	.114	.156	.163	.178	.185	.190	.278	.287	.302
28	.000	.000	.000	.000	.005	.004	.008	.012	.016	.016	.019	.025	.028	.035	.038	.046	.052	.057	.064	.066	.092	.098	.101	.108	.113	.167	.172	.181
29	.000	.000	.000	.005	.005	.004	.012	.020	.024	.024	.028	.038	.044	.054	.060	.075	.089	.096	.109	.119	.156	.170	.178	.184	.195	.282	.294	.307
30	.000	.000	.000	.000	.000	.004	.008	.012	.016	.016	.022	.025	.032	.038	.044	.052	.062	.068	.075	.084	.110	.119	.126	.134	.141	.202	.209	.215
31	.000	.000	.000	.005	.005	.008	.016	.020	.028	.032	.032	.041	.054	.063	.069	.084	.096	.107	.119	.132	.173	.186	.192	.206	.211	.311	.324	.336
34	.000	.000	.000	.000	.000	.000	.000	.000	.000	.004	.003	.003	.009	.009	.009	.014	.016	.021	.023	.025	.029	.033	.039	.040	.040	.059	.061	.064
35	.000	.000	.005	.005	.000	.004	.004	.012	.012	.012	.016	.019	.022	.025	.028	.032	.034	.041	.043	.048	.062	.065	.066	.072	.075	.104	.106	.112
36	.005	.005	.005	.010	.010	.012	.016	.016	.020	.024	.025	.032	.038	.044	.050	.055	.064	.068	.078	.087	.105	.112	.117	.126	.132	.173	.179	.188
37	.000	.000	.000	.000	.000	.000	.000	.000	.004	.004	.003	.006	.006	.013	.013	.016	.016	.018	.021	.023	.029	.032	.033	.035	.033	.052	.054	.058
38	.000	.000	.005	.005	.005	.004	.012	.016	.020	.020	.025	.035	.038	.044	.054	.059	.064	.073	.084	.091	.113	.121	.130	.135	.144	.198	.204	.215
39	.005	.005	.010	.015	.015	.016	.020	.028	.036	.044	.044	.057	.066	.079	.088	.100	.116	.132	.139	.157	.195	.206	.219	.230	.243	.327	.337	.352
40	.000	.000	.000	.000	.000	.000	.000	.004	.004	.004	.006	.009	.013	.016	.019	.021	.025	.027	.030	.032	.043	.047	.048	.051	.052	.076	.076	.082
41	.000	.000	.005	.005	.005	.004	.012	.016	.024	.024	.028	.035	.044	.050	.057	.068	.075	.087	.093	.105	.134	.144	.152	.161	.171	.235	.245	.253
42	.005	.010	.015	.020	.015	.016	.028	.040	.053	.057	.063	.076	.095	.110	.126	.141	.160	.180	.198	.221	.277	.293	.309	.327	.342	.465	.482	.503
48	.000	.000	.000	.000	.000	.000	.000	.000	.000	.000	.000	.000	.000	.000	.000	.007	.005	.005	.005	.005	.014	.012	.014	.015	.017	.020	.023	.023
49	.000	.000	.000	.000	.000	.000	.000	.000	.000	.000	.000	.003	.003	.006	.003	.011	.011	.014	.016	.016	.022	.022	.023	.025	.025	.038	.038	.041
50	.000	.000	.000	.000	.000	.004	.004	.008	.008	.008	.009	.013	.016	.019	.019	.021	.023	.025	.030	.034	.041	.044	.048	.048	.052	.074	.076	.080
51	.000	.000	.000	.000	.000	.000	.000	.000	.000	.000	.003	.003	.006	.006	.009	.016	.016	.018	.018	.021	.025	.026	.029	.029	.029	.046	.046	.045
52	.000	.000	.000	.000	.000	.000	.000	.004	.004	.004	.006	.013	.016	.016	.019	.021	.023	.027	.030	.032	.041	.043	.047	.050	.054	.073	.076	.080
53	.000	.000	.000	.000	.000	.004	.004	.012	.012	.016	.016	.019	.025	.032	.035	.039	.043	.052	.055	.062	.077	.084	.087	.092	.097	.137	.142	.148
54	.000	.000	.000	.000	.000	.000	.000	.000	.004	.004	.003	.009	.013	.016	.016	.018	.023	.023	.027	.030	.040	.040	.043	.044	.047	.072	.072	.077
55	.000	.000	.000	.000	.000	.000	.004	.008	.008	.012	.013	.016	.019	.025	.028	.034	.039	.041	.046	.050	.068	.072	.073	.080	.083	.118	.122	.126
56	.000	.000	.005	.005	.005	.008	.012	.016	.024	.024	.028	.035	.041	.050	.057	.064	.075	.084	.093	.103	.130	.141	.148	.159	.167	.231	.239	.250

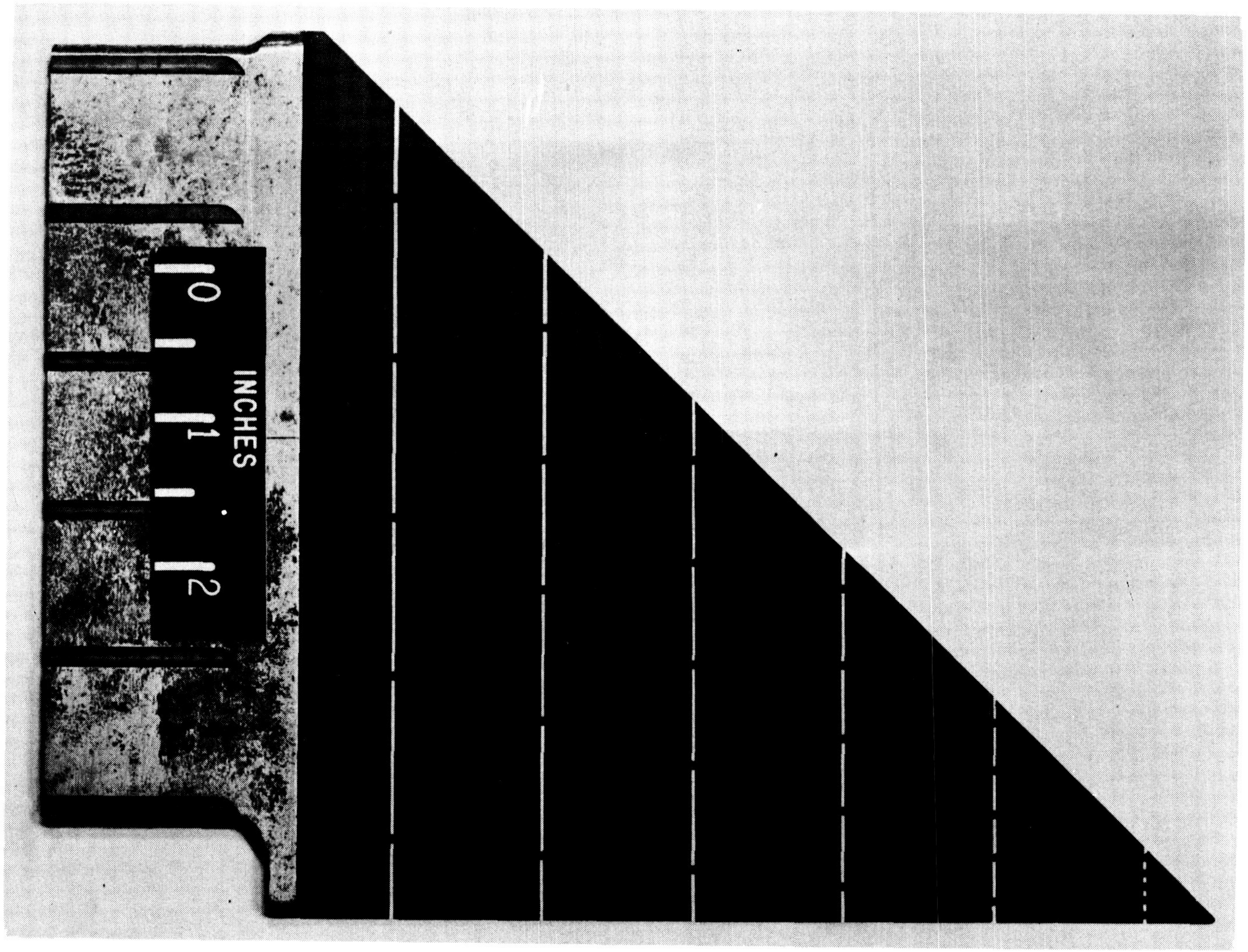

Figure 1.- Photograph of test model. L-61-2945

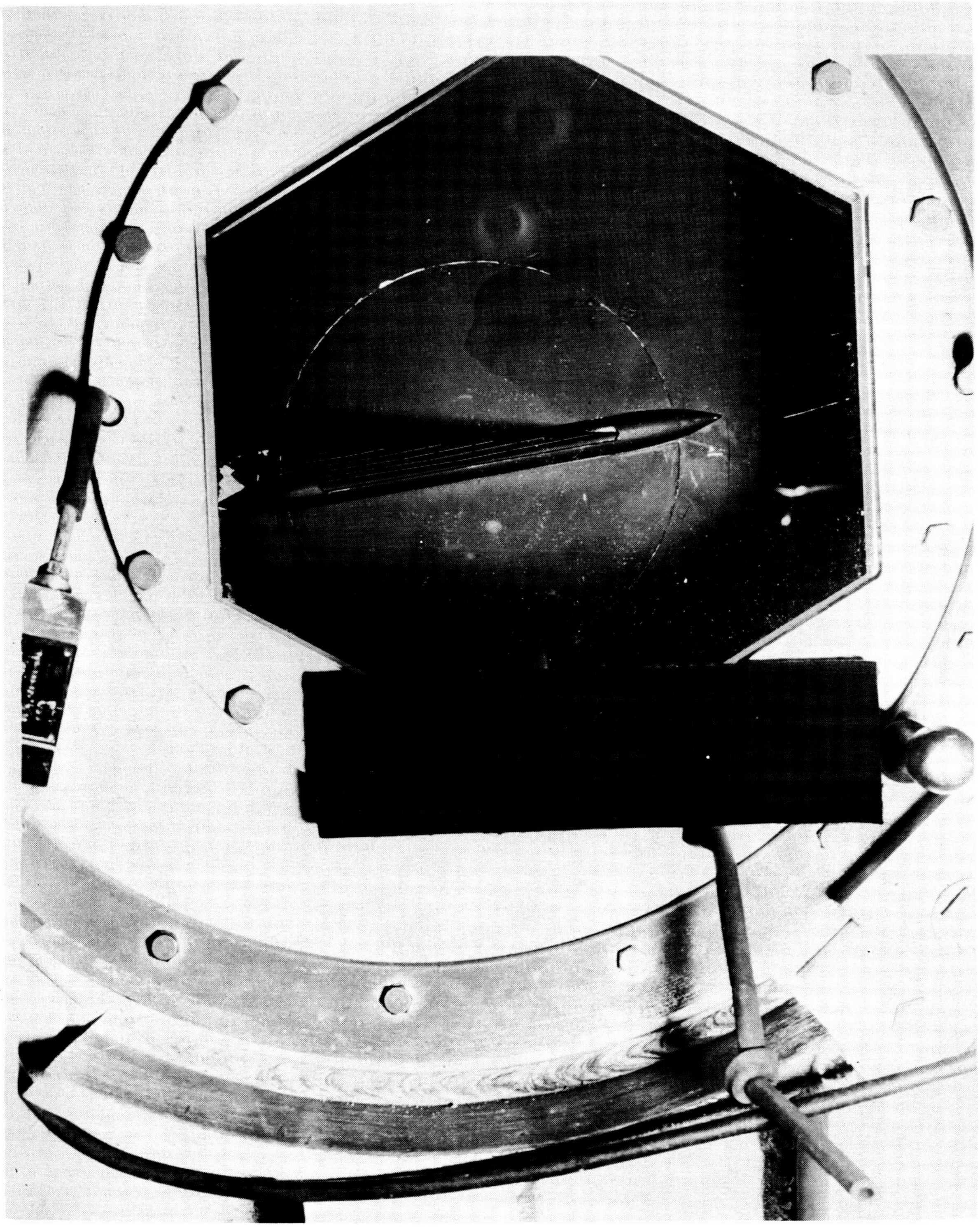

L-61-5073
Figure 2.- Model mounted in wind tunnel in undeformed position.

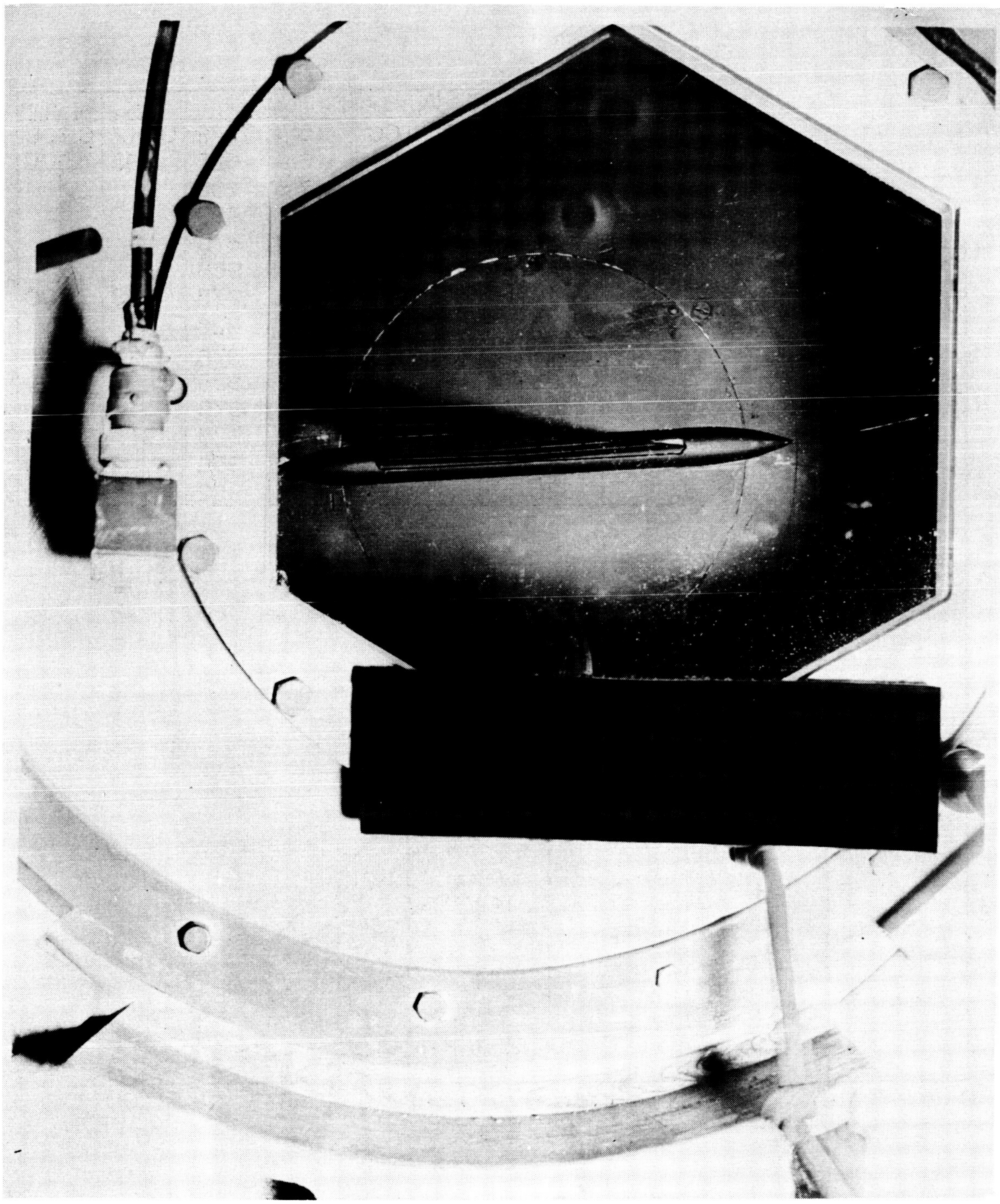

L-61-5074

Figure 3.- Double-exposure photograph of model in deformed and undeformed positions.

Station	$\bar{x}_i$	$\bar{y}_i$	A_i, sq in.	Station	$\bar{x}_i$	$\bar{y}_i$	A_i, sq in.
1	0.175	0.083	1.100	15	0.942	0.417	0.700
2	.358			16	.625	.583	.500
3	.542			17	.708		
4	.725			18	.792		
5	.908			19	.875		
6	.325	.250	.900	20	.958		
7	.475			21	.775	.750	.300
8	.625			22	.825		
9	.775			23	.875		
10	.925			24	.925		
11	.475	.417	.700	25	.975		
12	.592			26	.925	.917	.150
13	.708			27	.958		.200
14	.825			28	.992		.150

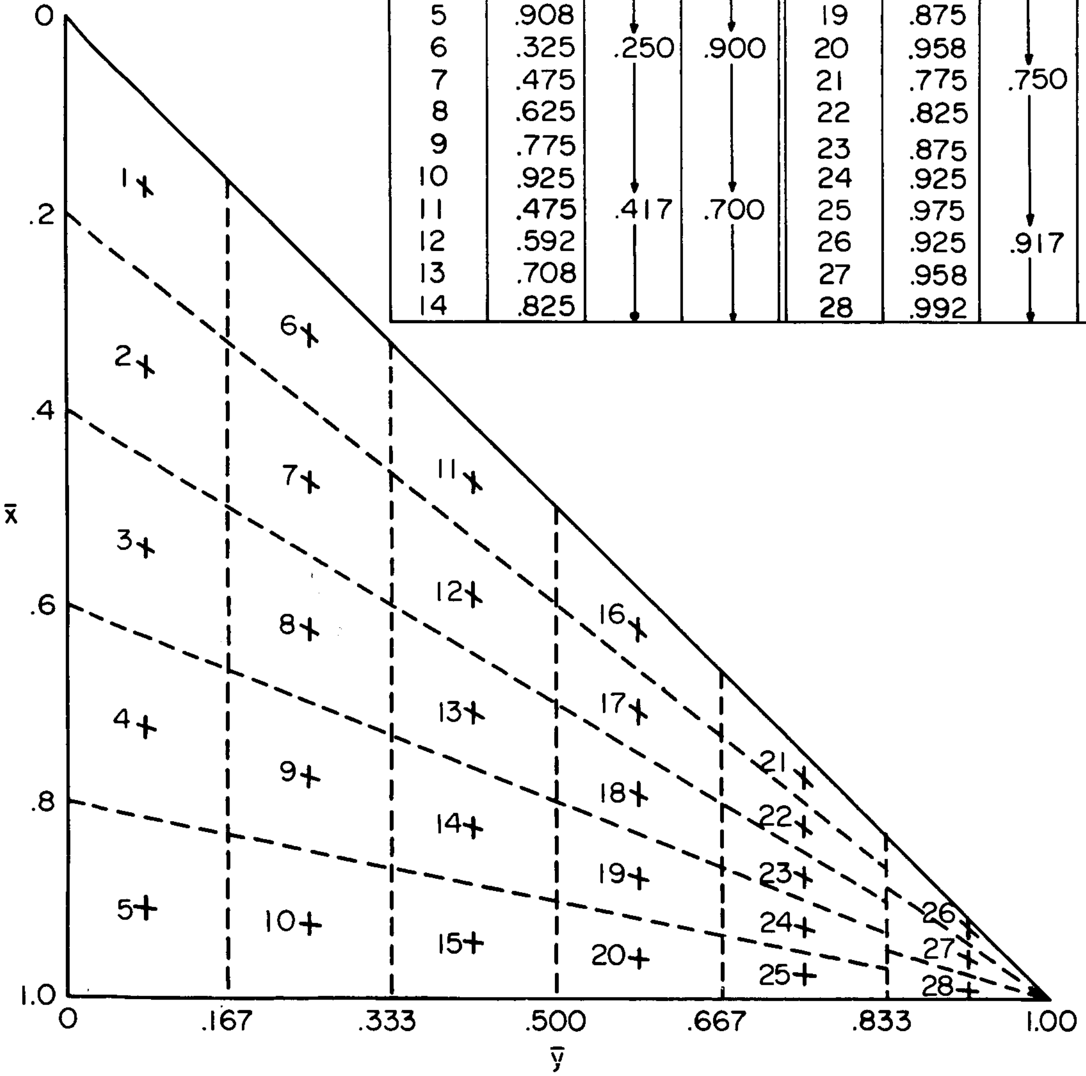

Figure 4.- Location of deflection stations and associated areas. Dashed lines represent boundaries of area segments.

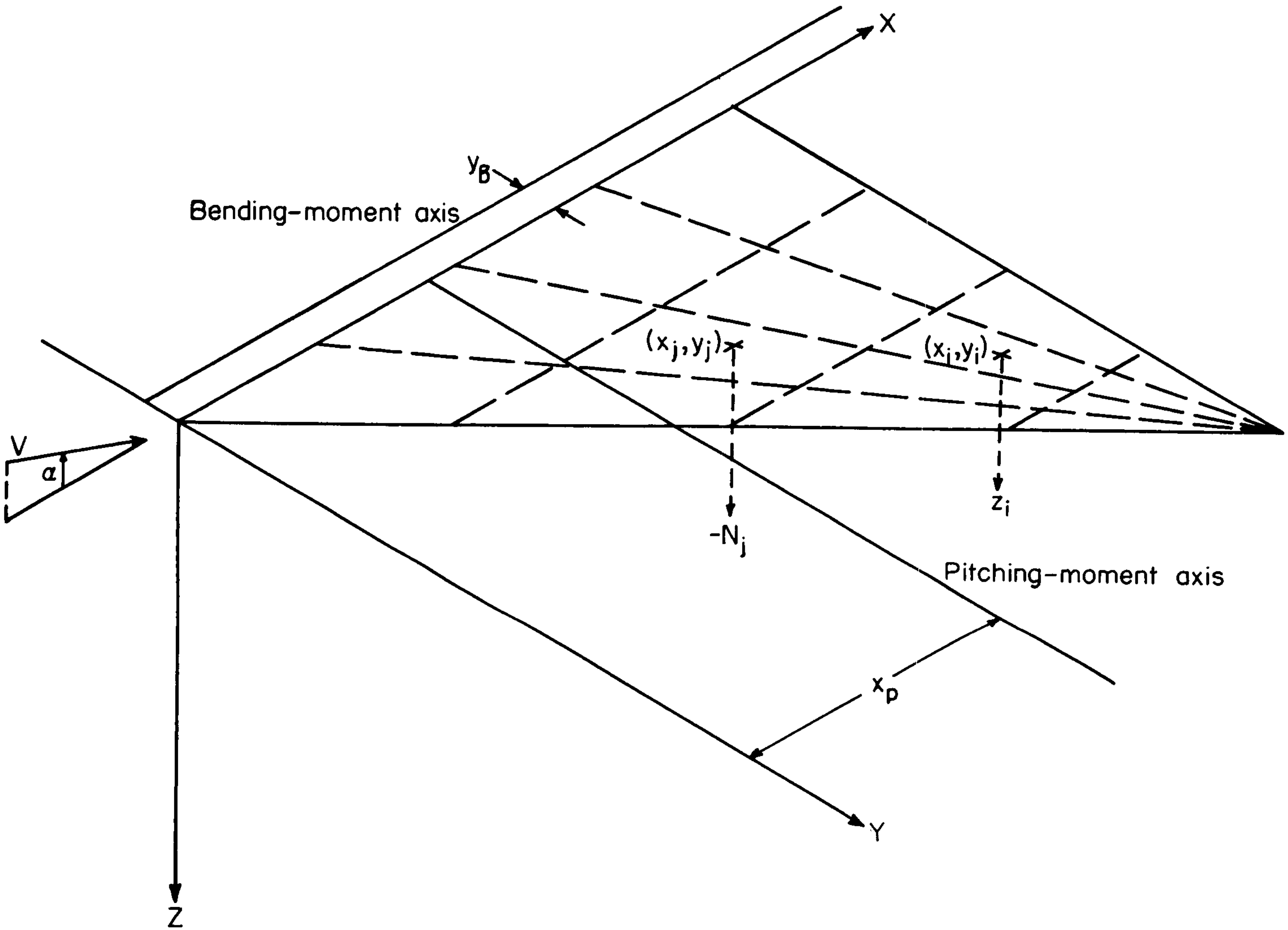

Figure 5.- Axis system.

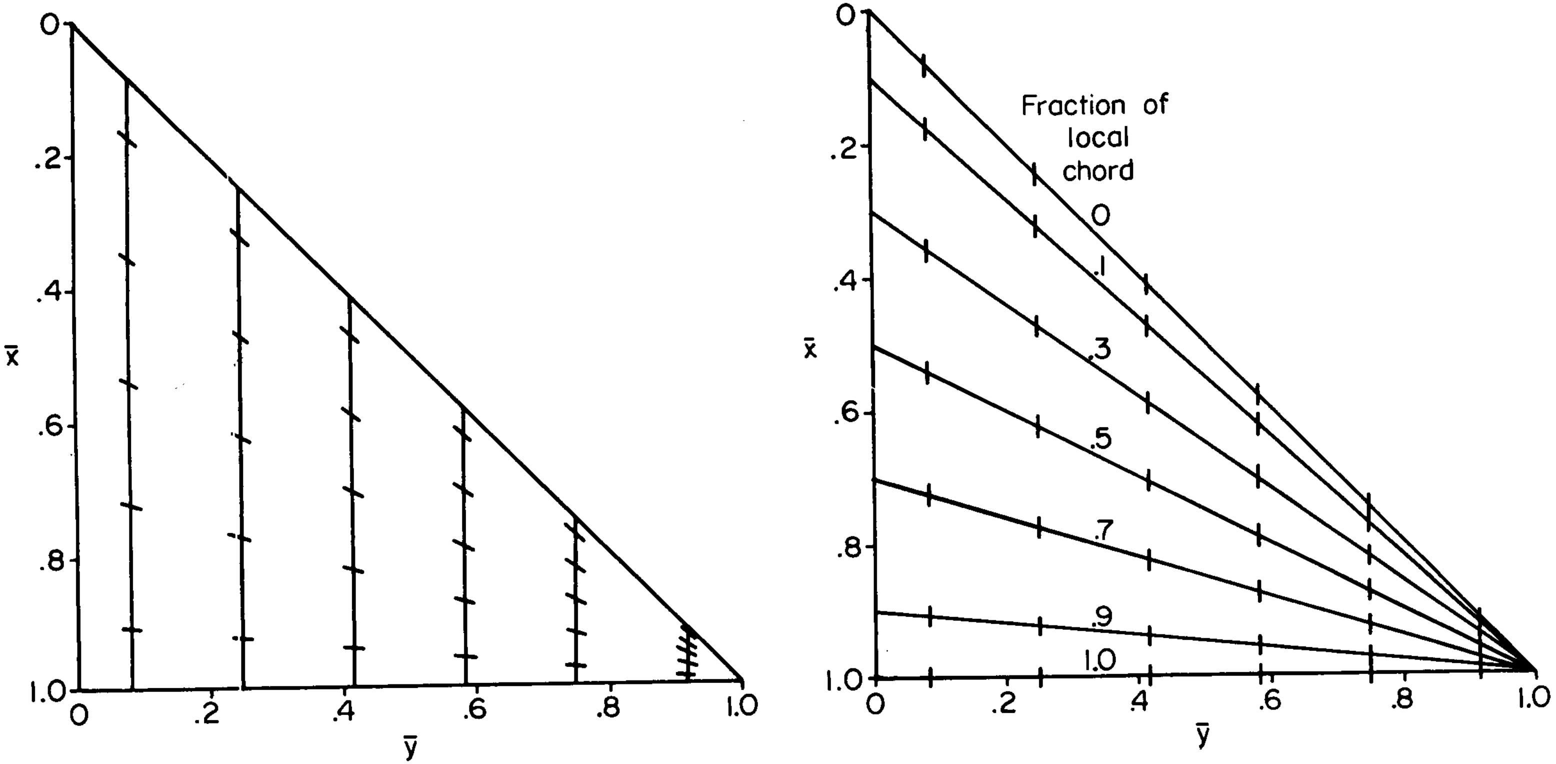

(a) Local chords.

(b) Span lines.

Figure 6.- Location of stations on local chords and on span lines for deformation plots.

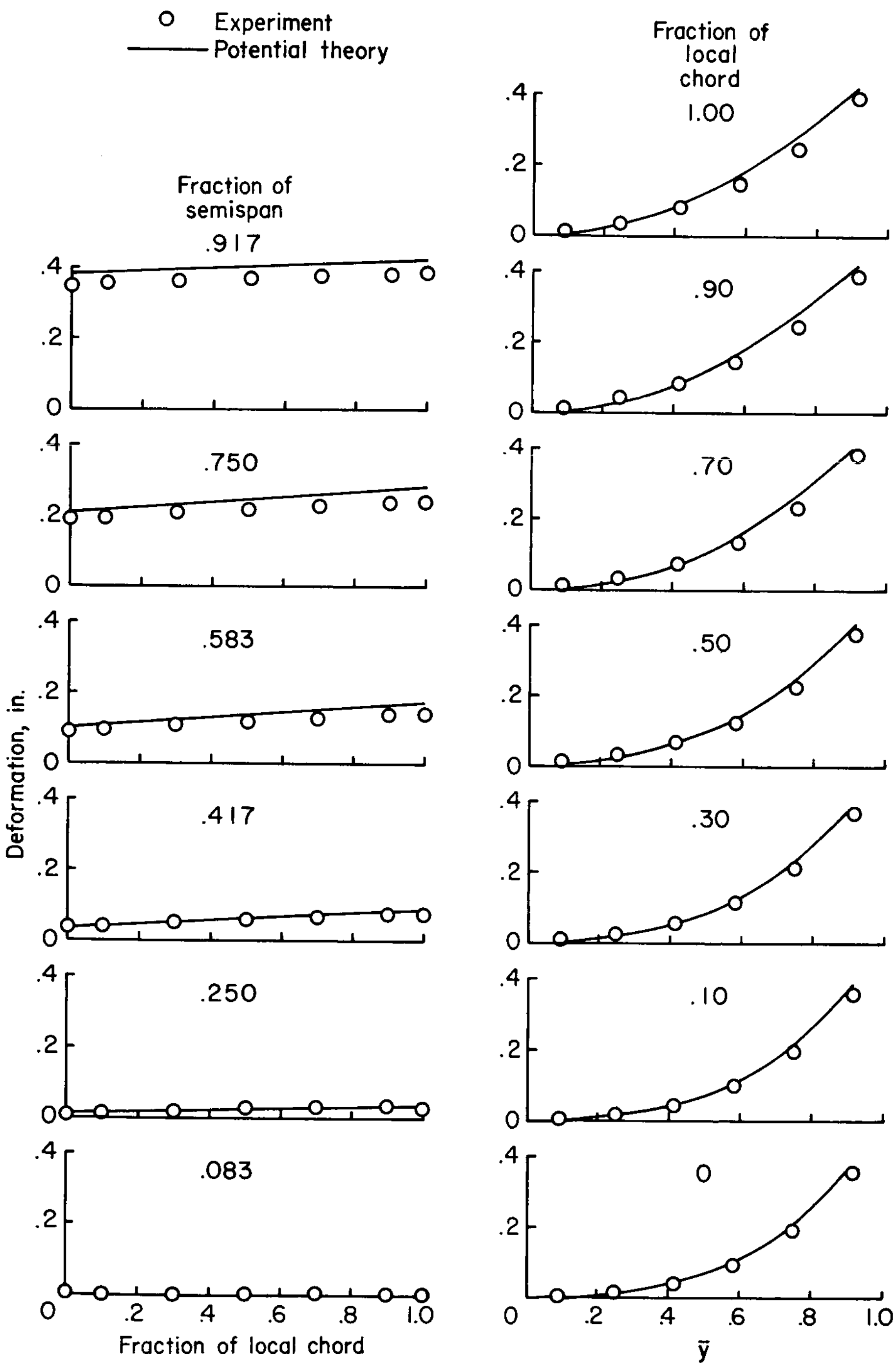

(a) $M = 1.30$; $\alpha = 4^{\circ}$; $q = 900$ lb/sq ft.

Figure 7.- Sample plots of wing deformations.

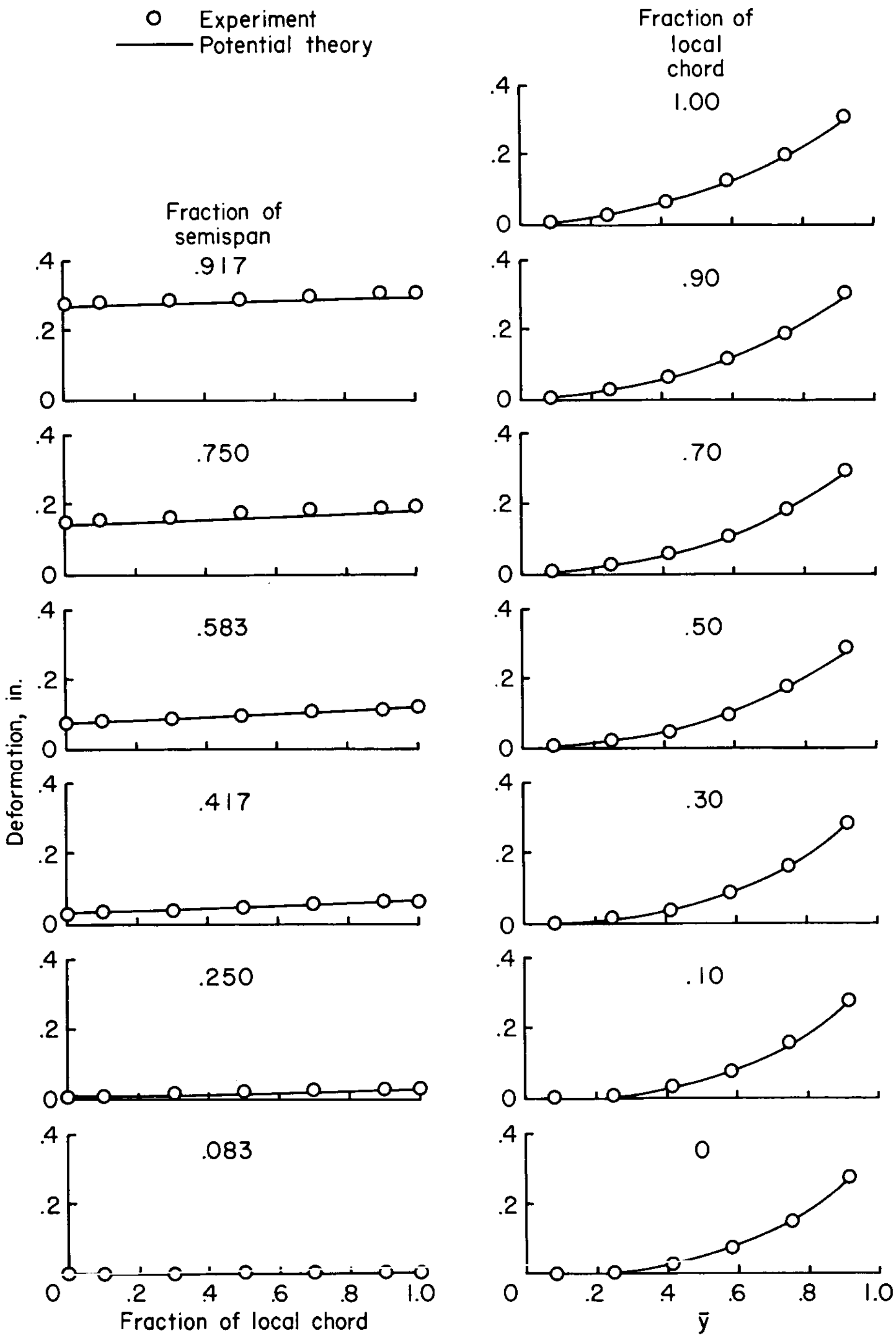

(b) M = 1.64; α = 4°; q = 999 lb/sq ft.

Figure 7.- Continued.

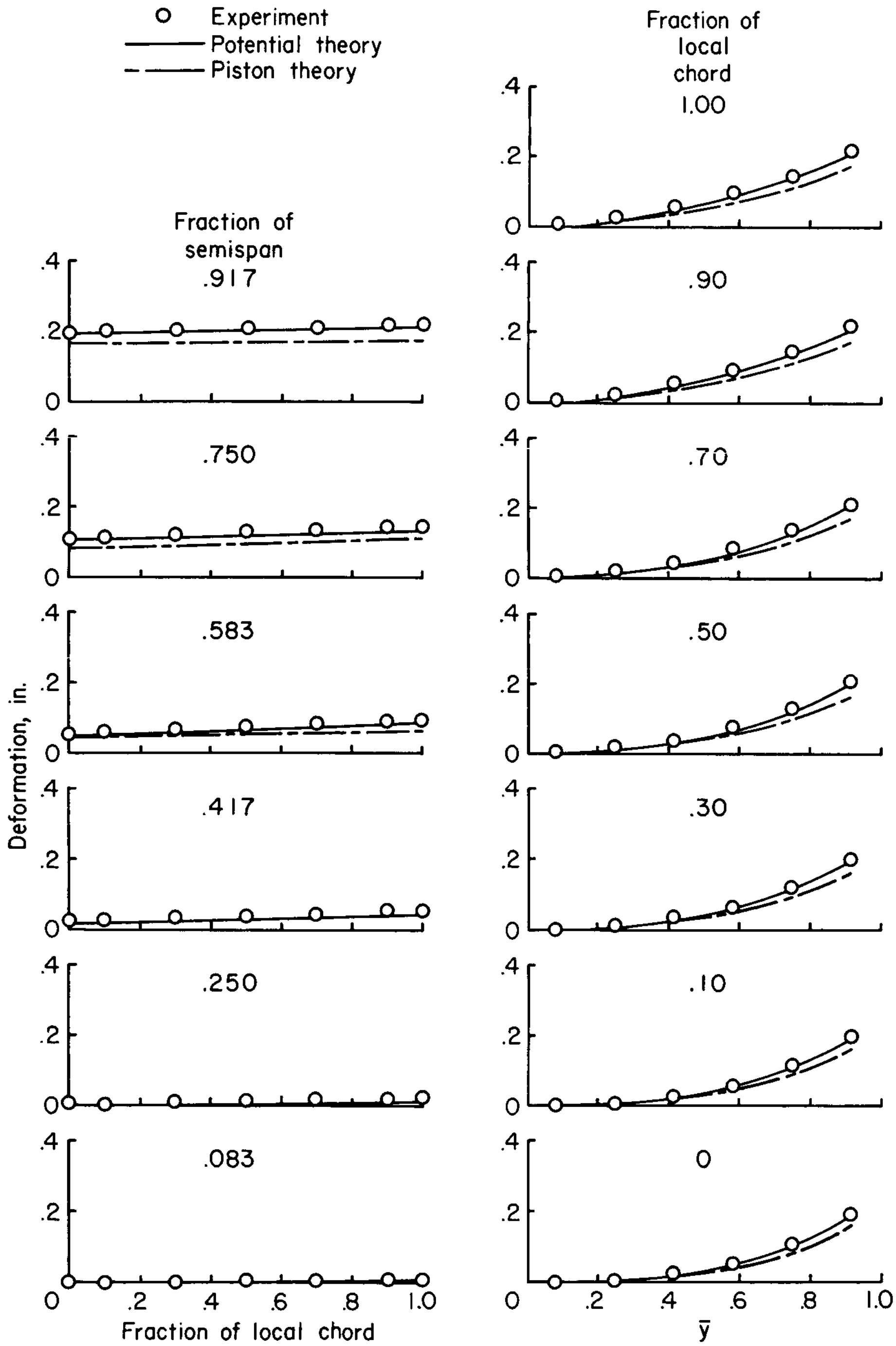

(c) M = 3.00; α = 6°; q = 1,055 lb/sq ft.

Figure 7.- Continued.

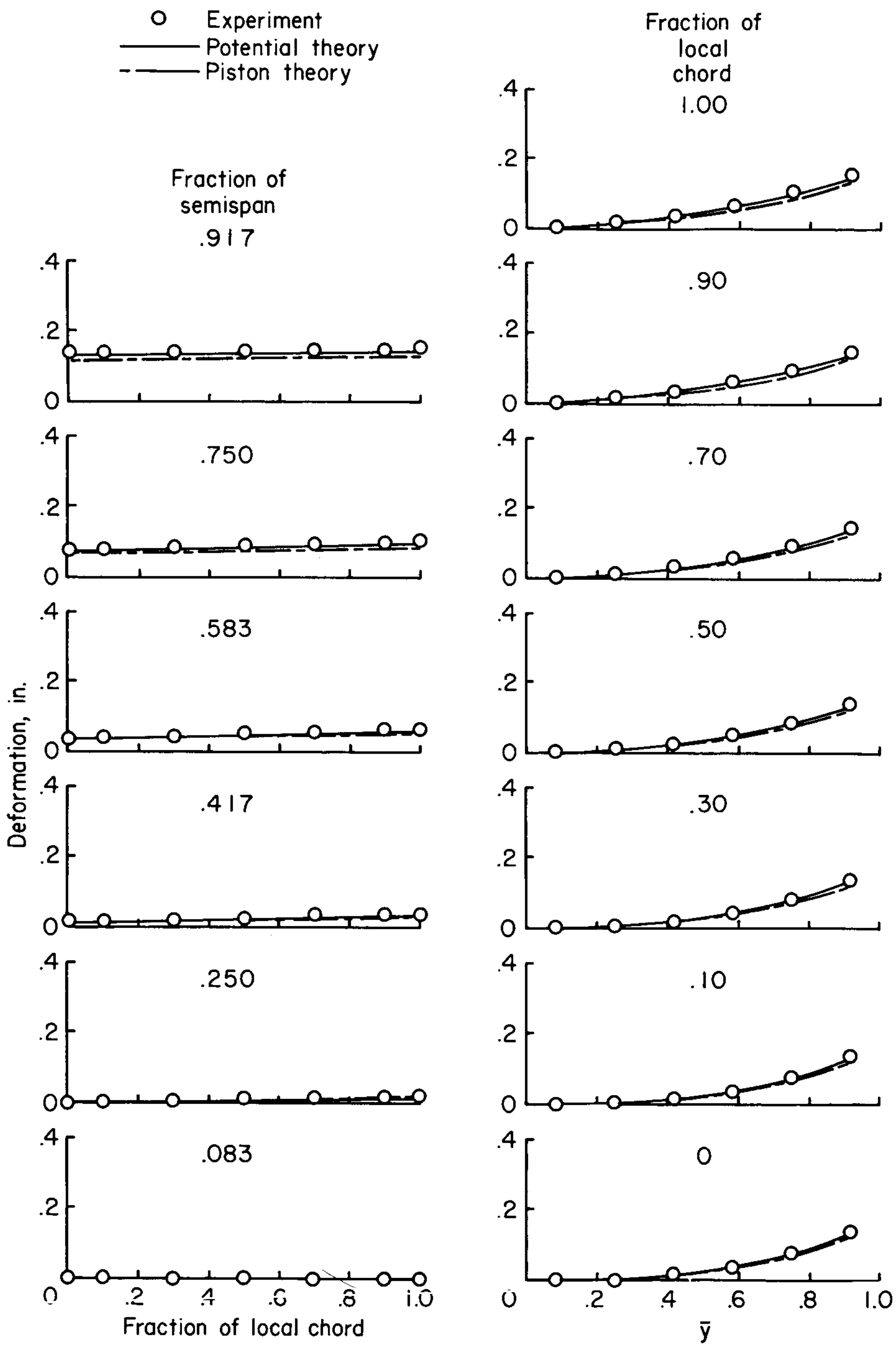

(d) $M = 4.00$; $\alpha = 6^{\circ}$; $q = 980$ lb/sq ft.

Figure 7.- Concluded.

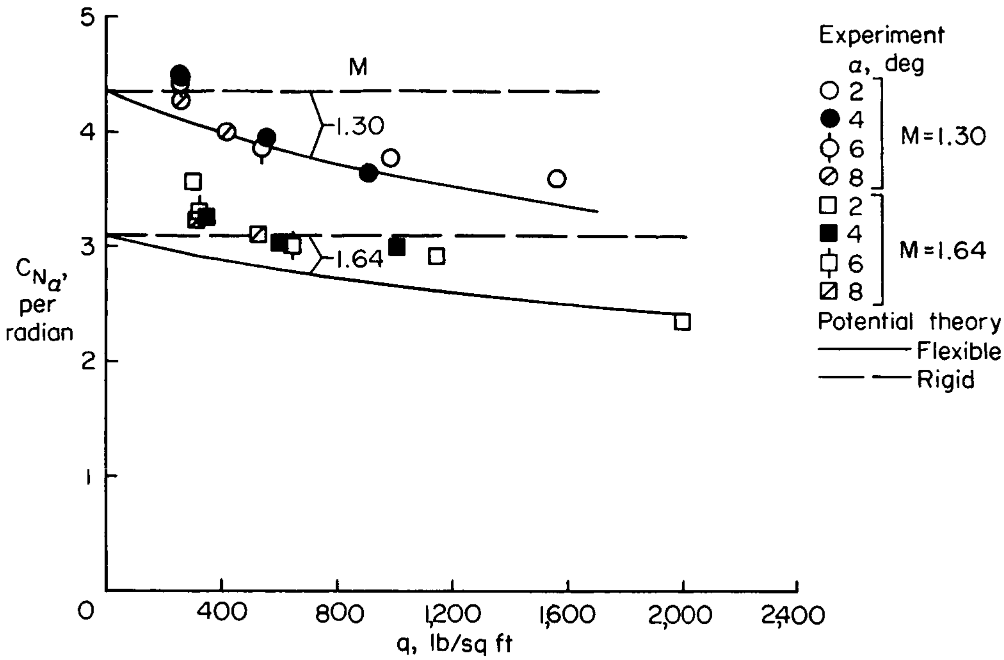

(a) Low Mach numbers.

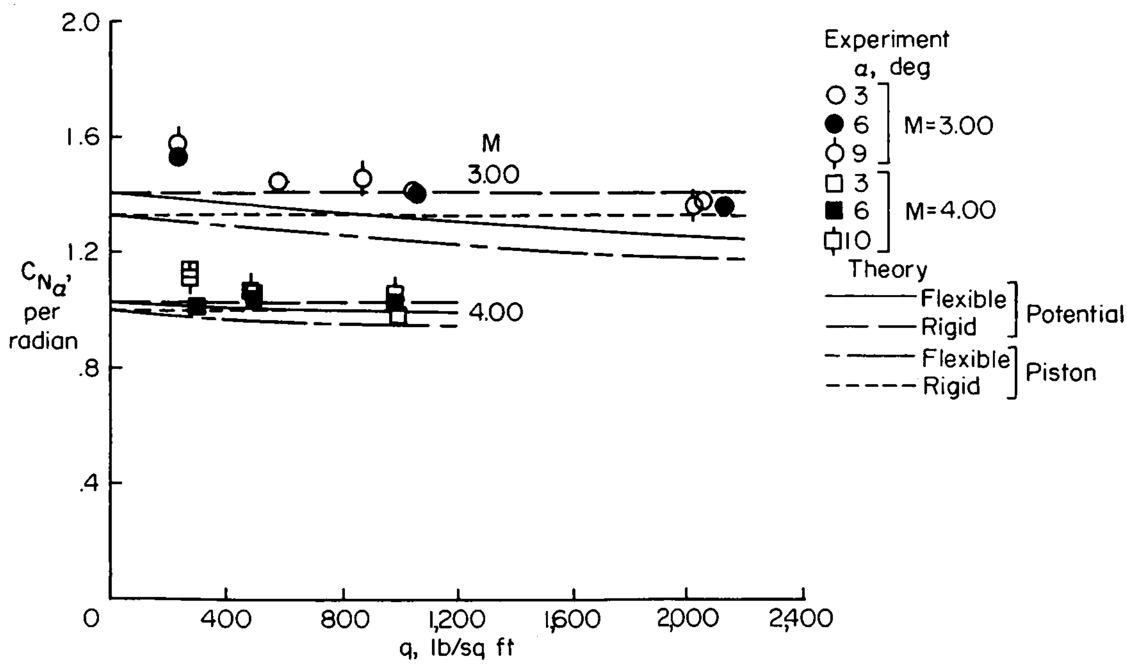

(b) High Mach numbers.

Figure 8.- Variation of normal-force coefficient per unit angle of attack with dynamic pressure.

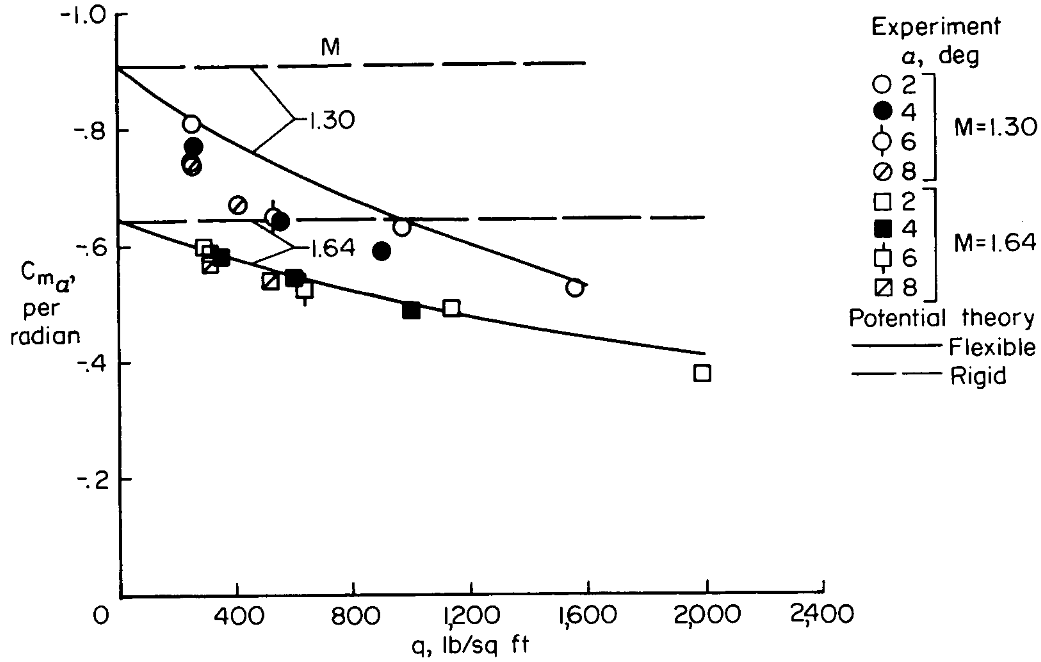

(a) Low Mach numbers.

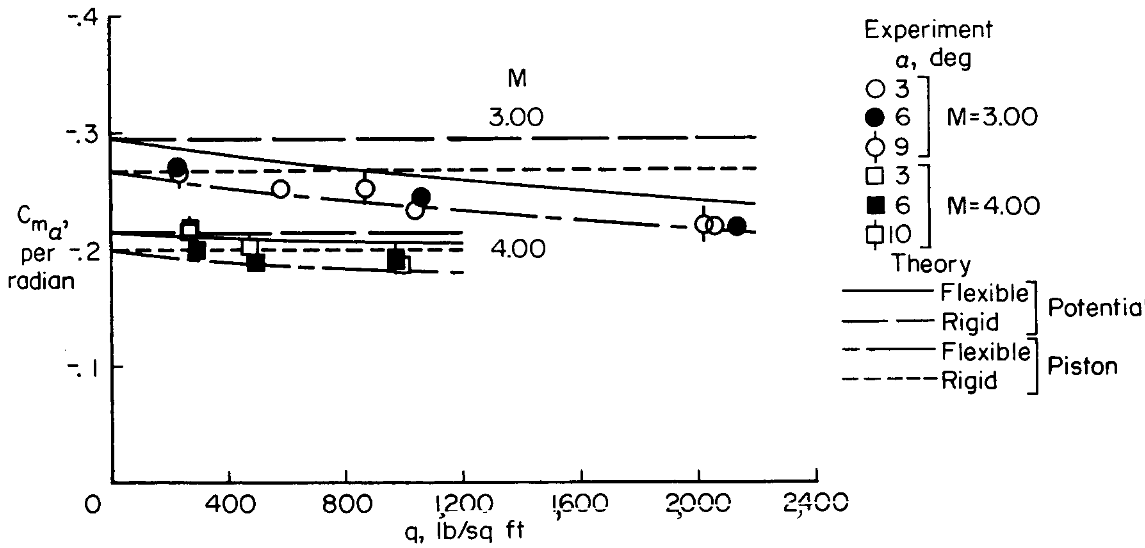

(b) High Mach numbers.

Figure 9.- Variation of pitching-moment coefficient per unit angle of attack with dynamic pressure.

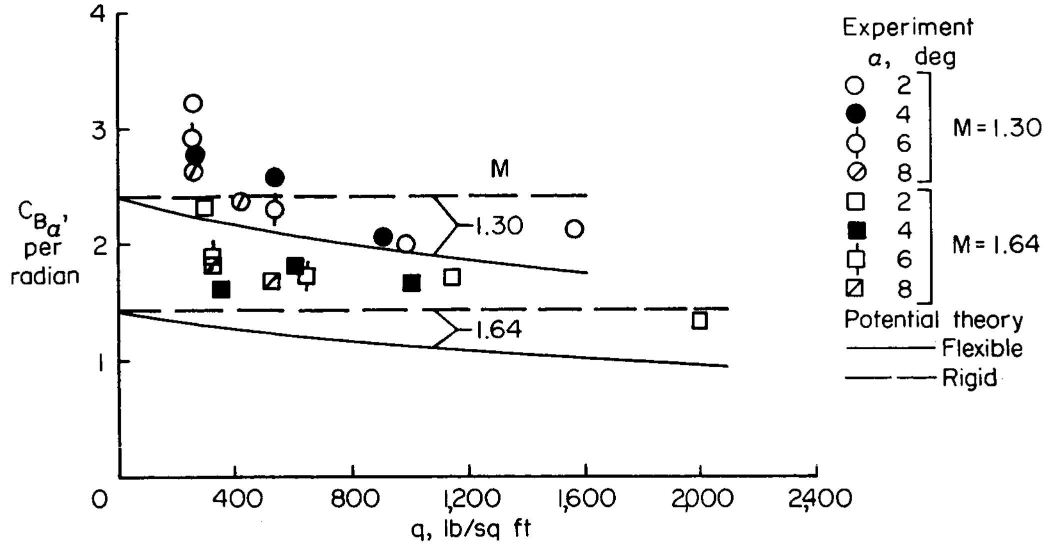

(a) Low Mach numbers.

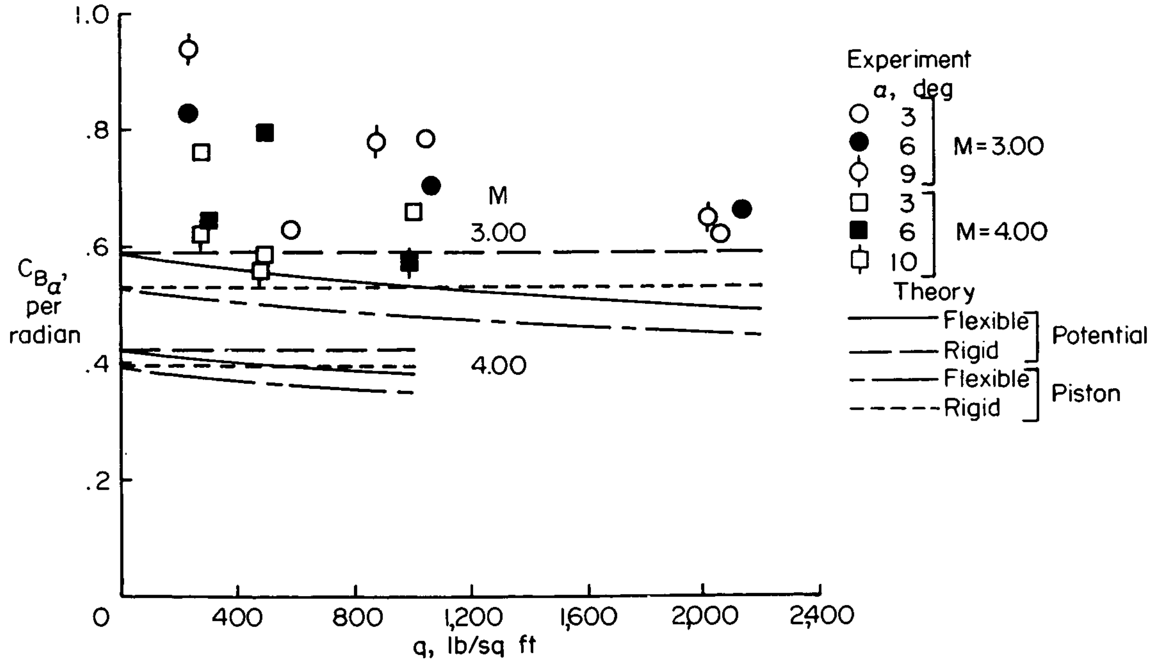

(b) High Mach numbers.

Figure 10.- Variation of bending-moment coefficient per unit angle of attack with dynamic pressure.